Signatures of the atomic structure in sub-femtosecond laser-driven electron dynamics in nanogaps

Luke Bhan,[1] Cody Covington,[2] and Kálmán Varga[1,*]

[1] *Department of Physics and Astronomy, Vanderbilt University, Nashville, Tennessee, 37235, USA*
[2] *Department of Chemistry, Austin Peay State University, Clarksville, USA*

(Dated: December 7, 2021)

Coupled Maxwell and quantum mechanical equations are used to simulate the electron dynamics in nanogaps in systems containing thousands of atoms. It will be shown that besides the carrier envelop phase (CEP), bow-tie or gap shape, and gap size, the atomistic structure also significantly alters the electron dynamics. Atomic-scale interference fringes appear not only in the electron density but in the electron current and field enhancement as well. Electron bursts emerge from individual atoms and scatter on atoms driven by the direction of the laser. The time-dependent orbital-free density functional theory coupled to the Maxwell equations allows us to simulate physical systems approaching the realistic size and to explore the physical mechanism controlling the electron dynamics.

I. INTRODUCTION

The precise control of the carrier-envelope phase (CEP) of few-cycle laser pulses at sub-femtosecond time scales allows the manipulation of charge carrier dynamics by the electromagnetic field of light [1–7]. By suitable choice of CEP, the oscillating electric field of a light wave can drive electrons across a nanoscale plasmonic gap several orders of magnitudes faster than the gigahertz speed of conventional electronics [8–17]. Bow-tie antennas are particularly useful because they can significantly increase the electron emission by resonant plasmonic effects [4, 15, 18–24]. The excited plasmons can induce strong, localized electric fields, which can drive large electron currents from the nanostructures [19, 25–30].

The electron transport between nanoparticles is controlled by several different factors. When the nanostructures are close to each other, their near fields couple leading to enhancement depending on the distance, shape, and size of the nanoparticles [31]. The electron dynamics also depend on the energy of the photons as well as the duration and CEP of the laser pulse.

To describe a realistic physical system, one needs to simulate thousands of atoms which is very difficult for quantum mechanical approaches. The time-dependent density functional theory (TDDFT) [32] is a common method of choice, but TDDFT based calculations either use jellium models neglecting atomic details [33–36] or are restricted to small model systems [37–44].

The importance of the atomic structure [38, 40] and the quantum effects [34] are well recognized and emphasized by the TDDFT calculations. For example, the individual atomic protrusions into the gap can significantly increase local electromagnetic enhancement in addition to the plasmonic fields [40, 45] and quantum phenomena, such as confinement and tunneling play an important role [34].

Another important physical mechanism is the coupling between electromagnetic fields and matter. The electron current and time-dependent charge oscillations induce electric fields in a highly nonlinear manner. In TDDFT and other quantum mechanical approaches this is usually neglected, while in electrodynamics simulation, the microscopic electron dynamics are not included. The external laser fields excite density oscillations and currents localized around the atoms and the latter, in turn, induced electric fields.

In this work, we will address both of these issues by coupling the atomistic quantum description of electron dynamics and the time-dependent electromagnetic fields to describe electron bursts and transport in plasmonic nanogaps. We will show, that besides the carrier envelop phase, bow-tie or gap shape, and gap size, the atomistic structure also substantially changes the electron dynamics. In the simulations, atomic-scale interference fringes appear not only in the electron density but in the electron current and field enhancement as well. Electron bursts emerge from individual atoms and scatter on atoms driven by the direction of the laser. This interference and scattering modulate the electron dynamics on the atomic scale.

Both the coupling between light and matter and the atomistic description is very important in understanding the dynamics of ultrafast electron currents in nanogaps. To address these for realistic physical devices one has to be able to simulate the electron dynamics in systems with thousands of atoms. For small model systems the effect of coupling between light and matter is small because there is not enough charges to create large induced fields. The orbital-free (OF) density functional theory (DFT) [46] is a good approach for large systems because its main variable is the electron density and it computationally scales linearly with system size, showing in million-atom material simulations [47]. We will use the time-dependent DFT version of the OF-DFT, the OF-TDDFT in our cal-

* kalman.varga@vanderbilt.edu

culations coupled with the Maxwell equations using the Riemann-Silbertsen vector in real space to describe the electromagnetic fields [48]. In previous work, we have shown that the currents and induced fields predicted by OF-TDDFT calculations are in very good agreement to TDDFT calculations using orbitals for jellium sheets, jellium spheres, atomistic sheets, and icosahedron clusters [49].

The OF-TDDFT equation is a time-dependent Schrödinger equation for a single orbital [49]

$$\left(i\hbar\frac{\partial}{\partial t} - H_{OF}\right)\Psi(\boldsymbol{r},t) = 0 \tag{1}$$

where

$$H_{OF}(\boldsymbol{r},t) = -\frac{1}{2m}[-i\hbar\nabla_{\boldsymbol{r}} + \boldsymbol{A}(\boldsymbol{r},t)]^2 + V_{OF}[\rho](\boldsymbol{r},t) \tag{2}$$

The density-dependent potential V_{OF} is defined in Ref. [50]. The electron density and the electron current at time t is defined as

$$\rho_{OF}(\boldsymbol{r},t) = |\Psi(\boldsymbol{r},t)|^2, \tag{3}$$

and

$$\boldsymbol{J}_{OF}(\boldsymbol{r},t) = 2\mathrm{Re}[\Psi(\boldsymbol{r},t)^*(-i\hbar\nabla_{\boldsymbol{r}} + \boldsymbol{A}(\boldsymbol{r},t))\Psi(\boldsymbol{r},t)]. \tag{4}$$

To solve the Maxwell equations we use the Reimann-Silberstein (RS), which is coupled to the OF-TDDFT equation by the method developed in Ref. [48]. In this approach, the RS vector is defined as

$$\boldsymbol{F}(\boldsymbol{r},t) = \sqrt{\frac{\epsilon_0}{2}}\boldsymbol{E}(\boldsymbol{r},t) \pm i\sqrt{\frac{1}{2\mu_0}}\boldsymbol{B}(\boldsymbol{r},t) \tag{5}$$

and this vector satisfies the Maxwell equations in the form

$$i\hbar\frac{\partial \boldsymbol{F}}{\partial t} = c\left(\boldsymbol{S}\cdot\frac{\hbar}{i}\nabla_{\boldsymbol{r}}\right)\boldsymbol{F} - \frac{i\hbar}{\sqrt{2\epsilon_0}}\boldsymbol{J} \tag{6}$$

where $\boldsymbol{S}$ are the spin-1 3×3 Pauli matrices. The main advantage of this approach is that Eq. (6) is similar to a time-dependent Schrödinger-equation (see Eq. (1)).

The wavefunction is represented on a real-space grid and is time propagated using Taylor time evolution. A more detailed description can be found in Ref. [49]. In the numerical calculation, first, the ground state wave function is calculated by diagonalizing H_{OF} on a real space grid, which is taken to be the wavefunction at $t = 0$. An external laser pulse is added to the system of the form

$$E_z(\boldsymbol{r},t) = E_0\sin(\omega(t-x/c)+\phi)e^{-(t-t_0-x/c)^2/\alpha^2}\Gamma(t) \tag{7}$$

where $\Gamma(t)$ is a ramping function that ensures the electric field is zero at $t = 0$, α is the carrier-envelope width, ω is the field frequency, E_0 is the field strength and ϕ is the carrier-envelope phase. The external field is turned on and creates a vector potential that drives electron motion. Eqs. (6) and (1) are solved on a real-space grid of the same grid spacing by time-propagation. The parameters of the laser pulse and the pulse shape for different carrier-envelope phases are shown in Ref. [50]. The details of the numerical solution of the coupled equations are given in [50].

We will use aluminum bow-tie structures similar to the one in Fig. 1 to study the electron dynamics in nanogaps. The two main variables of this geometry are the distance between the tips and the bow-tie angle (see Ref. [50]). Aluminum bow-tie structures are considered good alternatives [51–53] to noble metal (gold and silver) bow-ties and their field enhancement properties have been investigated experimentally [22, 52, 54, 55] and by finite-difference time-domain (FDTD) simulations [56–59]. The field enhancement in the gap is found to be between 20 and 100 [56, 57, 59] depending on the geometry of the structure. This is somewhat smaller than the field enhancement in gold bow-tie antennas [4, 20].

In the simulations, the electric field from the laser drives electron density to the tips of the bow tie, which creates a strong induced electric field around the tip. Snapshots of the electron density, electron current, and electric field are shown in Fig. 1 for $\phi = 0$. In these figures (6000 atoms and 18000 electrons are used in this example), the fingerprint of the underlying atomic structure can clearly be seen in the density, current and electric field. The electron current is emitted not only from the tip atoms but from a wider region and the absorption extends into layers of atoms. This is even more clearly visible in the excited state density ($\rho(t) - \rho(0)$) where the charge density on individual atoms deep inside the tips varies with the electric field (see Fig. 1c). The snapshots in Fig. 1c clearly demonstrate that the electron transport and dynamics evolve through excitation of individual atoms.

The induced electric field (Fig. 1d) and electron current (Fig. reffig:bowtie1e) also changes on atomic scale in space. Fig. 1d shows that the electric field is strong inside the tips and interference like fringes are present, which is commensurate with the atomic structure. The figures also show that the electric fields and currents change sign between atoms or atomic layers corroborating that the atomic structure is important and strongly influences the electron dynamics.

Fig. 1f shows the field enhancement at a frequency $\omega = 1$, where the enhancement is the largest. The bright spots correspond to an enhancement of a factor of 40-45. There is a bright hot spot along the line that connects the two tips and reaches inside the tip region deep inside the atomic layers. where two small hot spots can also be seen.

To analyze the flow of electrons from one tip to another, the flux of electrons through a given surface are calculated as

$$\Phi(t) = -\Delta t\int dxdy\mathrm{J}_z(\boldsymbol{r},t), \qquad \Phi_T = \int_0^T dt\Phi(t). \tag{8}$$

Fig. 2a shows the flux of electrons between the tips. The

surface is taken to be the xy plane which lies in between the two structures. When the laser field is symmetric ($\phi = 0$), it moves the electrons from one tip to the other and back leading to a net transfer across the bowtie of close to zero. The amplitude of the laser field reaches its first maxima at around $t = 30$ a.u. and the second one, with the opposite sign at $t = 45$a.u. The flux follows this oscillation with a 20 a.u. time delay. The figure also shows the importance of coupling the Maxwell and OF-TDDFT equations. In the uncoupled case, the induced fields due to the dynamics of electrons are neglected and the flux is about two times bigger than in the coupled case. We also considered the effect of system size on the flux. Fig. 2 shows that the time dependence of the flux for a smaller system [50] is very similar to that of the larger system, but the flux transfer is somewhat smaller.

The number of transported electrons from one tip to the other strongly depends on the CEP. Fig. 2b shows the flux for different ϕ values between 0 and 2π. CEP values of $\phi = \pi/2$ and $\phi = 3\pi/2$ have the largest net electron transport, and they move the electrons in the opposite directions, as dictated by the symmetry of the laser. In this case, the maximum transfer is 0.5 electrons over a time frame of 70 atomic units of time corresponding to a current of $50\mu A$. which is very large. The field enhancement (see Fig. 2c) seems to have very small dependence on the CEP.

Next, we study the effect of gap size on the electron transport between the tips. In these simulations, the distance between the tips is varied and the same laser was used as before with CEP of $\phi = 0$. The gap size is defined as the distance between the outermost atoms on the tips. As expected, with a larger gap size, there is a smaller induced field amplitude and thus a smaller field enhancement (Fig. 2e). In particular, for approximately every 2 a.u. (0.1 nm) increase in gap size, there is a 10 percent drop in the overall enhancement.

Fig. 2f) shows that the net electron transport between the tips strongly depend on the gap distance. This is because the large gap size inhibits the electrons from moving back when the laser changes direction because there is a time delay in the transport process. The larger the gap, the farther the electrons have to travel, meaning the electron packet does not make it across the gap before the laser field reverses. This example shows that one can use the gap size to control the electron transfer between tips.

The appeal of the bowtie system with a single pulsed asymmetric laser is that electron transport can occur without a bias. However, it is still worth exploring the amplification of transport by a bias as it is commonly used in chip technologies. These calculations have the same laser as before, but the external field is biased by a voltage that is equal to a certain percentage of the maximum laser amplitude, E_0, for the entire duration of the simulation. We utilize bias voltage values of 0.016 (8.39 V/nm), 0.032 (16.78 V/nm), 0.049 (25.16 V/nm), 0.065 (33.56 V/nm), and 0.082 (41.95 V/m); ranging between 10 to 50 percent of E_0. The larger the bias, the larger the field amplitude, however, there is a new oscillation when compared to a non biased field at time $t = 15$ to $t = 30$, shown in Fig. 3b. In the non-biased case (Fig. 2a), there is no flux before $t = 30$and this new peak is due to the bias. Fig. 3a shows that the bias significantly increases the field enhancement. This is the consequence of the increased electron current in the gap region (Fig. 3a), especially for large biases. Additionally, the electron transfer, shown in Fig. 3c, continues in the direction of the bias as long as the bias stays active even after the laser pulse and as expected, these are much larger fluxes than in the non-biased case. Fig. 3d shows the flux as the function of time. One can see that flux is driven by the electric field (see Fig. 3b and 3c), but there is a time delay between the two.

In the following, we explore another possibility to asymmetrically transfer electrons across the gap using a multicolor laser shown in Fig. 3e. A combination of two wavelengths of frequencies of ω and 2ω is used in this pulse (for definition see Ref. [50]). Fig. 3f shows that the field flux is still similar to the single-color pulse laser despite reaching a much higher laser amplitude (almost 0.27 a.u. as shown in Fig. 3e compared to 0.19 in the case of the single pulse). The biggest effect of the two-color laser is that it changes the CEP dependence of the flux. The largest flux is at $\phi = 0$ and $\phi = \pi$ while the single pulsed laser had the largest flux at $\phi = \frac{\pi}{2}$. The most interesting effect of the multicolor laser is that it can be used to change the direction of the electron current. For example, using $\phi = \frac{\pi}{2}$ with a single color laser the net electron flow is from the upper tip to the lower tip (Fig. 2b). By turning on the second laser (Fig. 3f) the electrons will flow in the opposite direction.

Finally, we have also investigated bow-tie structures with asymmetric tips (see Fig. 4). Asymmetric structures have the potential for net electron transport for all values of CEP. Several different geometries were investigated. In asymmetric sharp-blunt bowtie structures, the field enhancement does not significantly change (Fig. 4), but using different shapes, one can steer the current from the sharper tip to the wider tip even with $\phi = 0$. The field enhancement around a single tip (without the other tip) is about 1/3 of the field enhancement of the asymmetric structures, so even a flat surface increases the field enhancement in the gap. Fig. 4 shows that the current now flows in one direction outward the tip. This geometry allows sending electron packets from the sharp tip to a wider tip or to a sheet controlled by the laser without relying on the CEP.

In summary, coupled OF-TDDFT Maxwell simulations have been performed on aluminum bowtie systems comprised of thousands of atoms. Atomistic features appear in the time-dependent electron densities, currents and induced electric fields indicating the importance of the atomistic description. These OF-TDDFT calculations substantially extend the applicability of quantum mechanical simulations and the atomistic simulation of realistic devices are within the reach of this approach. We

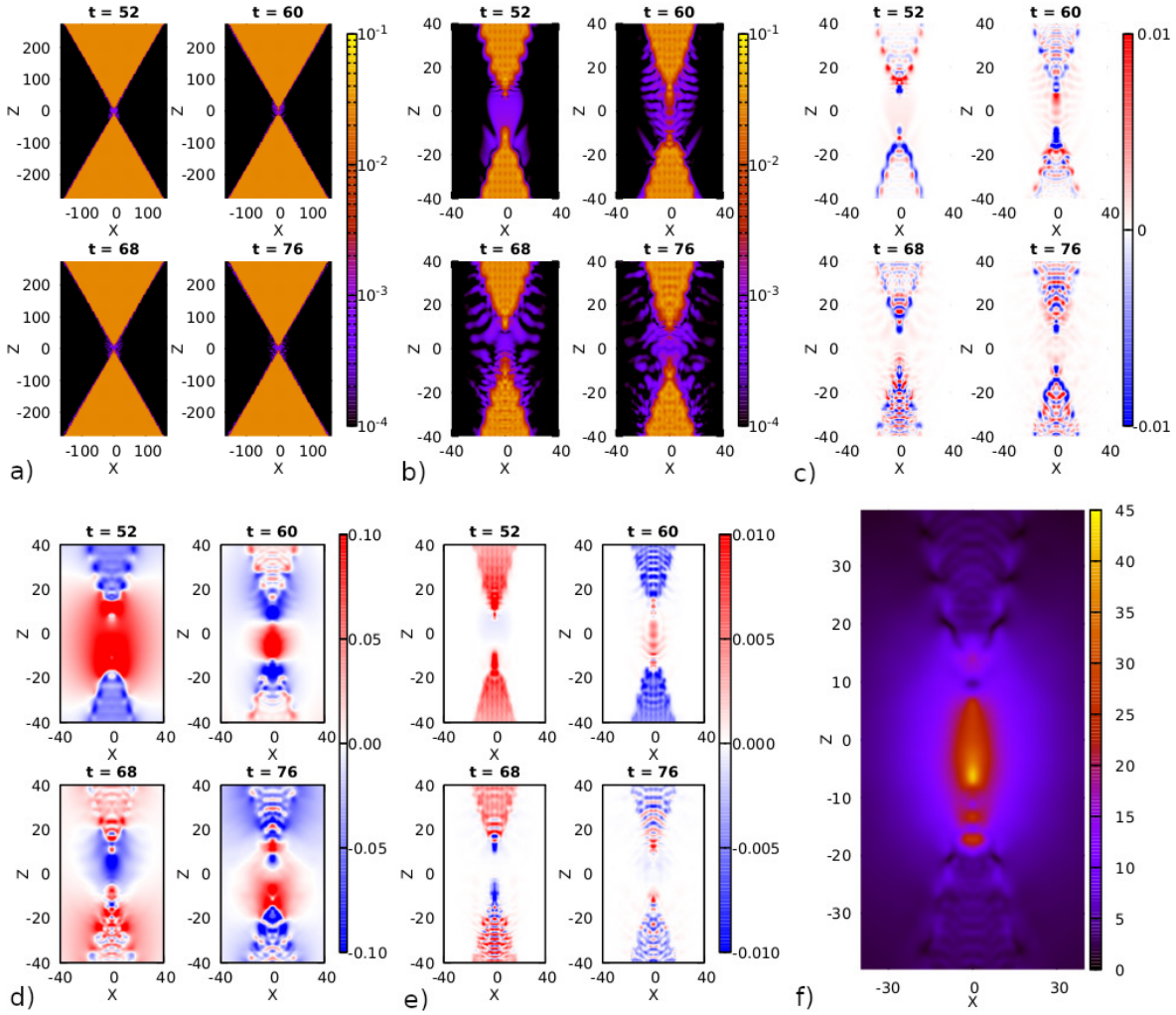

FIG. 1. Electron density (a), electron density in the gap region (b), excited-state electron density, $\rho(t) - \rho(0)$, in the gap region (c), electric field in the gap (d) current in the gap (e) and field enhancement in the gap (f) in a bowtie structure. The figures are obtained by averaging over the y direction. 6000 atoms with 18000 electrons are used.

have shown that unidirectional currents can be generated in several different ways, like with optimized CEP, with multicolor laser, or by using asymmetric bow-tie structures. These atomistic coupled OF-TDDFT Maxwell simulations might be useful in the investigation of various nanoscale devices where the interaction of electromagnetic fields and matter is important.

[1] M. Hentschel, R. Kienberger, C. Spielmann, G. A. Reider, N. Milosevic, T. Brabec, P. Corkum, U. Heinzmann, M. Drescher, and F. Krausz, Nature **414**, 509 (2001).

[2] E. Goulielmakis, V. S. Yakovlev, A. L. Cavalieri, M. Uiberacker, V. Pervak, A. Apolonski, R. Kienberger, U. Kleineberg, and F. Krausz, Science **317**, 769 (2007), https://science.sciencemag.org/content/317/5839/769.full.pdf.

[3] F. Krausz and M. Ivanov, Rev. Mod. Phys. **81**, 163 (2009).

[4] P. Dombi, Z. Pápa, J. Vogelsang, S. V. Yalunin, M. Sivis, G. Herink, S. Schäfer, P. Groß, C. Ropers, and C. Lienau, Rev. Mod. Phys. **92**, 025003 (2020).

[5] M. Krüger, C. Lemell, G. Wachter, J. Burgdörfer, and P. Hommelhoff, Journal of Physics B: Atomic, Molecular and Optical Physics **51**, 172001 (2018).

[6] J. J. Baumberg, J. Aizpurua, M. H. Mikkelsen, and D. R. Smith, Nature Materials **18**, 668 (2019).

[7] J. Lee, D.-J. Jeon, and J.-S. Yeo, Advanced Materials **n/a**, 2006606, https://onlinelibrary.wiley.com/doi/pdf/10.1002/adma.202006606.

[8] M. Ludwig, G. Aguirregabiria, F. Ritzkowsky, T. Rybka, D. C. Marinica, J. Aizpurua, A. G. Borisov, A. Leiten-

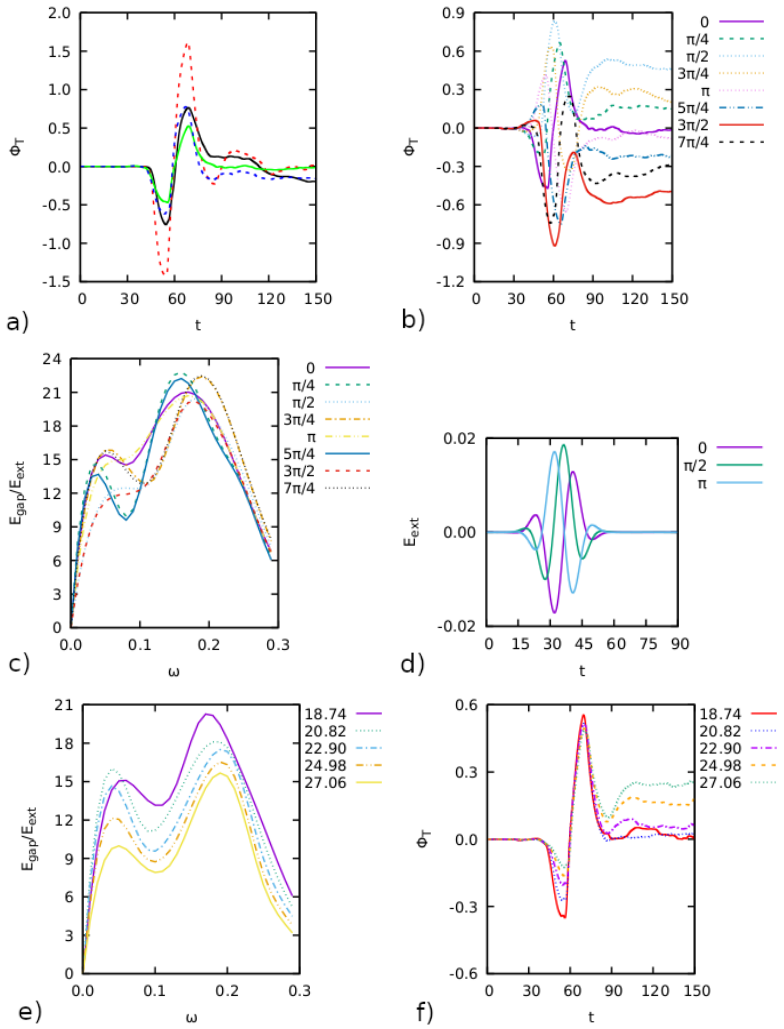

FIG. 2. Fluxes and field enhancements for various carrier-envelope phases. (a) Fluxes in two systems of different sizes (small and medium) are compared. The parameters defining the systems are listed in [50]. The dashed red line is the flux without, the solid black line is the flux with coupling in the medium-sized system. The dashed blue line is the flux without, the solid green line is the flux with coupling in the small system. (b) Fluxes for different carrier-envelope phases. (c) Field enhancements for different carrier-envelope phases. (d) Laser field for different CEPs. (e) Enhancement and (f) flux for different gap sizes.

storfer, and D. Brida, Nature Physics **16**, 341 (2020).
[9] L. Shi, I. Babushkin, A. Husakou, O. Melchert, B. Frank, J. Yi, G. Wetzel, A. Demircan, C. Lienau, H. Giessen, M. Ivanov, U. Morgner, and M. Kovacev, Laser & Photonics Reviews **15**, 2000475 (2021), https://onlinelibrary.wiley.com/doi/pdf/10.1002/lpor.202000475.
[10] M. Ludwig, A. K. Kazansky, G. Aguirregabiria, D. C. Marinica, M. Falk, A. Leitenstorfer, D. Brida, J. Aizpurua, and A. G. Borisov, Phys. Rev. B **101**, 241412 (2020).
[11] D. Buckley, Y. Yang, Y. Yang-Keathley, K. K. Berggren, and P. D. Keathley, J. Opt. Soc. Am. B **38**, C11 (2021).
[12] Y. Yang, M. Turchetti, P. Vasireddy, W. P. Putnam, O. Karnbach, A. Nardi, F. X. Kärtner, K. K. Berggren, and P. D. Keathley, Nature Communications **11**, 3407 (2020).
[13] M. R. Bionta, F. Ritzkowsky, M. Turchetti, Y. Yang, D. Cattozzo Mor, W. P. Putnam, F. X. Kärtner, K. K. Berggren, and P. D. Keathley, Nature Photonics **15**, 456 (2021).
[14] M. Turchetti, M. R. Bionta, Y. Yang, F. Ritzkowsky, D. R. Candido, M. E. Flatté, K. K. Berggren, and P. D. Keathley, J. Opt. Soc. Am. B **38**, 1009 (2021).
[15] T. Rybka, M. Ludwig, M. F. Schmalz, V. Knittel, D. Brida, and A. Leitenstorfer, Nature Photonics **10**, 667 (2016).
[16] C. Karnetzky, P. Zimmermann, C. Trummer, C. Duque Sierra, M. Wörle, R. Kienberger, and A. Holleitner, Nature Communications **9**, 2471 (2018).
[17] G. M. Rossi, R. E. Mainz, Y. Yang, F. Scheiba, M. A. Silva-Toledo, S.-H. Chia, P. D. Keathley, S. Fang, O. D. Mücke, C. Manzoni, G. Cerullo, G. Cirmi, and F. X. Kärtner, Nature Photonics **14**, 629 (2020).
[18] W. P. Putnam, R. G. Hobbs, P. D. Keathley, K. K. Berggren, and F. X. Kärtner, Nature Physics **13**, 335 (2017).
[19] R. G. Hobbs, W. P. Putnam, A. Fallahi, Y. Yang, F. X.

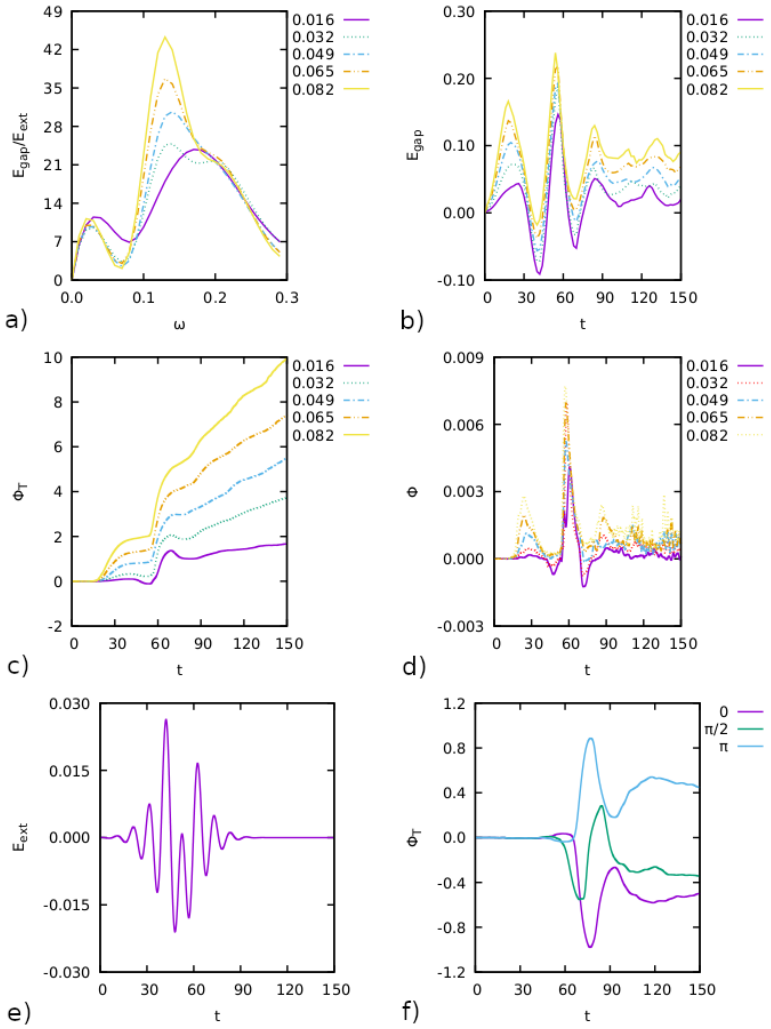

FIG. 3. Field enhancement(a), electric field (b), flux (c), and flux at time t (d) for a biased laser pulse. Laser (e) and fluxs of multiple CEPs (f) for two-colored laser pulses

Kärtner, and K. K. Berggren, Nano Letters **17**, 6069 (2017), pMID: 28926275.

[20] P. J. Schuck, D. P. Fromm, A. Sundaramurthy, G. S. Kino, and W. E. Moerner, Phys. Rev. Lett. **94**, 017402 (2005).

[21] M. Parzefall and L. Novotny, Reports on Progress in Physics **82**, 112401 (2019).

[22] B. Cerjan, X. Yang, P. Nordlander, and N. J. Halas, ACS Photonics **3**, 354 (2016).

[23] M. Runge, D. Engel, M. Schneider, K. Reimann, M. Woerner, and T. Elsaesser, Opt. Express **28**, 24389 (2020).

[24] A. Bhattacharya, G. Georgiou, S. Sawallich, C. Matheisen, M. Nagel, and J. Gómez Rivas, Phys. Rev. B **93**, 035438 (2016).

[25] P. Dombi, A. Hörl, P. Rácz, I. Márton, A. Trügler, J. R. Krenn, and U. Hohenester, Nano Letters **13**, 674 (2013), pMID: 23339740.

[26] H. Robatjazi, S. Bahauddin, C. Doiron, and I. Thomann, Nano Letters **15** (2015), 10.1021/acs.nanolett.5b02453.

[27] C. M. Scheffler, R. C. Word, and R. Könenkamp, Plasmonics **16**, 371 (2021).

[28] Y. Shen, H. Chen, N. Xu, Y. Xing, H. Wang, R. Zhan, L. Gong, J. Wen, C. Zhuang, X. Chen, X. Wang, Y. Zhang, F. Liu, J. Chen, J. She, and S. Deng, ACS Nano **13**, 1977 (2019), pMID: 30747519.

[29] P. Zimmermann, A. Hötger, N. Fernandez, A. Nolinder, K. Müller, J. J. Finley, and A. W. Holleitner, Nano Letters **19**, 1172 (2019).

[30] K. Takano, M. Asai, K. Kato, H. Komiyama, A. Yamaguchi, T. Iyoda, Y. Tadokoro, M. Nakajima, and M. I. Bakunov, Scientific Reports **9**, 3280 (2019).

[31] J. Heimerl, T. Higuchi, M. Ammon, M. A. Schneider, and P. Hommelhoff, Phys. Rev. B **101**, 125403 (2020).

[32] E. Runge and E. K. U. Gross, Phys. Rev. Lett. **52**, 997 (1984).

[33] D. C. Marinica, A. K. Kazansky, P. Nordlander, J. Aizpurua, and A. G. Borisov, Nano Letters **12**, 1333 (2012).

[34] W. Zhu, R. Esteban, A. G. Borisov, J. J. Baumberg, P. Nordlander, H. J. Lezec, J. Aizpurua, and K. B. Crozier, Nature Communications **7**, 11495 (2016).

[35] G. Aguirregabiria, D.-C. Marinica, M. Ludwig, D. Brida, A. Leitenstorfer, J. Aizpurua, and A. G. Borisov, Fara-

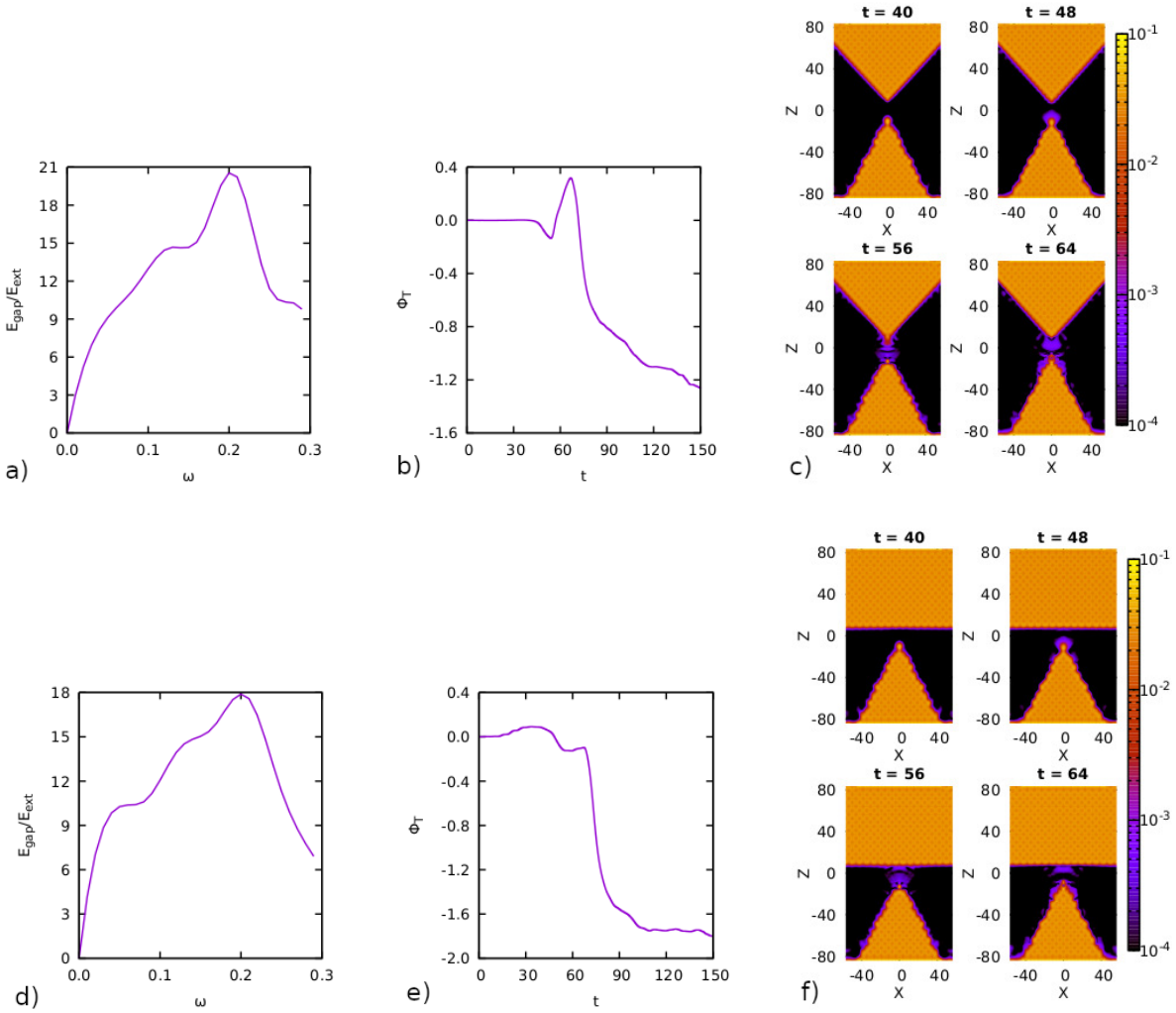

FIG. 4. Field enhancement (a)(d), flux (b)(e), and density snapshots (c)(e) in asymmetric bowtie structures. The CEP is $\phi = 0$.

day Discuss. **214**, 147 (2019).

[36] T. V. Teperik, P. Nordlander, J. Aizpurua, and A. G. Borisov, Phys. Rev. Lett. **110**, 263901 (2013).

[37] K. Uchida and K. Watanabe, Phys. Rev. B **96**, 125419 (2017).

[38] P. Zhang, J. Feist, A. Rubio, P. García-González, and F. J. García-Vidal, Phys. Rev. B **90**, 161407 (2014).

[39] A. Varas, P. García-González, F. J. García-Vidal, and A. Rubio, The Journal of Physical Chemistry Letters **6**, 1891 (2015), pMID: 26263265.

[40] M. Barbry, P. Koval, F. Marchesin, R. Esteban, A. G. Borisov, J. Aizpurua, and D. Sánchez-Portal, Nano Letters **15**, 3410 (2015), pMID: 25915173.

[41] R. Jestädt, M. Ruggenthaler, M. J. T. Oliveira, A. Rubio, and H. Appel, Advances in Physics **68**, 225 (2019).

[42] M. Kuisma, A. Sakko, T. P. Rossi, A. H. Larsen, J. Enkovaara, L. Lehtovaara, and T. T. Rantala, Phys. Rev. B **91**, 115431 (2015).

[43] E. Makkonen, T. P. Rossi, A. H. Larsen, O. Lopez-Acevedo, P. Rinke, M. Kuisma, and X. Chen, The Journal of Chemical Physics **154**, 114102 (2021).

[44] G. Giannone and F. Della Sala, The Journal of Chemical Physics **153**, 084110 (2020).

[45] F. Marchesin, P. Koval, M. Barbry, J. Aizpurua, and D. Sánchez-Portal, ACS Photonics **3**, 269 (2016).

[46] W. C. Witt, B. G. del Rio, J. M. Dieterich, and E. A. Carter, Journal of Materials Research **33**, 777 (2018).

[47] L. Hung and E. A. Carter, Chemical Physics Letters **475**, 163 (2009).

[48] C. Covington, D. Kidd, H. Buckner, H. Appel, and K. Varga, Phys. Rev. E **100**, 053301 (2019).

[49] C. Covington, J. Malave, and K. Varga, Phys. Rev. B **103**, 075119 (2021).

[50] See Supplemental Material.

[51] M. W. Knight, N. S. King, L. Liu, H. O. Everitt, P. Nordlander, and N. J. Halas, ACS Nano **8**, 834 (2014), pMID: 24274662.

[52] S. Ambardar, D. Nguyen, G. Binder, Z. W. Withers, and D. V. Voronine, Applied Sciences **10** (2020), 10.3390/app10124210.

[53] D. Gérard and S. K. Gray, Journal of Physics D: Applied Physics **48**, 184001 (2014).

[54] L. Li, S. Fang Lim, A. A. Puretzky, R. Riehn, and H. D. Hallen, Applied Physics Letters **101**, 113116 (2012).
[55] T. D. Dao, C. V. Hoang, N. Nishio, N. Yamamoto, A. Ohi, T. Nabatame, M. Aono, and T. Nagao, Micromachines **10** (2019), 10.3390/mi10070468.
[56] B. Wang, S. C. Singh, H. Lu, and C. Guo, Plasmonics **15**, 609 (2020).
[57] H. Fischer and O. J. F. Martin, Opt. Express **16**, 9144 (2008).
[58] A. Mohammadi, V. Sandoghdar, and M. Agio, Journal of Computational and Theoretical Nanoscience **6**, 2024 (2009).
[59] G. H. Chan, J. Zhao, G. C. Schatz, and R. P. Van Duyne, The Journal of Physical Chemistry C **112**, 13958 (2008).